1 Theoretical astrophysics

....

2 High energy astrophysics

2.1 CRT

....

2.2 Imaging Atmospheric Cherenkov Telescopes at La Palma

F. Aharonian, A. Akhperjanian[a], V. Aseykin, A. Daum, M. Hemberger, G. Hermann, M. Hess, A. Heusler, W. Hofmann, R. Kankanian[a], C. Köhler, A. Kohnle, A. Konopelko[b], T. Kutter, M. Panter, A. Plyasheshnikov[b], G. Pühlhofer, M. Ulrich, H.J. Völk, C. Wieland, C.A. Wiedner, H. Wirth

[a]Physics Institute, Yerevan, Armenia
[b]Altai State University, Barnaul, Russia

2.2.1 Introduction

The investigation of Cosmic Rays and of TeV γ-rays from cosmic sources with Imaging Air Cherenkov Telescopes represents one of the major activities of the laboratory in the field of experimental high-energy astrophysics. In 1995 the activities of the Heidelberg CT group concentrated along three lines of work:

- The continued participation in the observation program with the existing telescopes, including shift and analysis work.
- The main effort concentrated on the new system of five high resolution Imaging Cherenkov Telescopes. The central instrument, CT-3, was tested in Heidelberg, shipped to La Plama and started data taking in September. Since then the production of the other system telescopes is under way. The newly developed software for data acquisition and steering allows to control the full system.
- Considerable work went into the development of analysis tools, such as the procedures to combine the information of several telescopes observing the same shower, or to extract the full information from the recorded pictures. This work of course involves a large amount of detailed Monte Carlo simulations. At the time the system of five telescopes is running, the group will be prepared to exploit its full power.

2.2.2 Evolution and running of CT-1 and CT-2

The first (prototype) HEGRA telescope CT-1 with equatorial mount, $5\,\mathrm{m}^2$ reflector consisting of 18 spherical glass mirrors (thickness 2 cm, diameter 60 cm, and focal length $f \approx 5\,\mathrm{m}$) and a 37-channel camera (pixel size 0.43° and field of view (FoV) $\approx$ 3°) has been installed and is taking data since 1992 [1]. In December 1994 the 37-channel camera was replaced by a new high resolution 127-channel camera with pixel size 0.25° and FoV$\approx$ 3.25°. The new 19 mm diameter photomultipliers from EMI have higher quantum efficiency than the photomultipliers (Soviet FEU-130) used in the previous camera: about 26% instead of 19% at a wavelength $\lambda = 350\,\mathrm{nm}$. In addition, the plexiglass light guides facing the mirrors have been replaced by open light collectors. This not only improves the light collection efficiency, but also decreases the sensitivity of the camera to stray background light. The Kiel group, responsible for this work, has implemented several new features, in particular a system for computer controlled setting of the high voltages of PMTs.

The second HEGRA telescope, CT-2, was installed in December 1993. It has an alt-azimuth mount and a reflector with 30 mirrors of a total area $8.5\,\mathrm{m}^2$. The camera in the focal plane consists of 61 closely packed photomultipliers FEU-130, with an angular size of each pixel 0.43°, and FoV$\approx$ 3.9°. The PMTs are optically coupled to plexiglass light guides having the shape of a hexagonal truncated cone. This telescope is described in the Institute's Annual Report for 1994 [2].

The observation program of 1995 concentrated on six astrophysical objects: the Crab Nebula, the AGN Mrk 421, the SNR G78.2+2.1 (γ-Cygni), the X-ray binary Cygnus X-3, the cataclysmic variable AE Aquarii, and the superluminal galactic source GRS 1915+105. Also, there were several attempts to detect VHE γ-ray signals shortly after γ-ray bursts seen by the BATSE detector on board the Compton GRO which were announced through the BACODINE network. Most of the time CT-1 and CT-2 were operating in stereoscopic observation mode, though due to some technical problems of timing and tracking, only limited observation periods are available for stereoscopic reconstruction of showers.

Below we present the results on the detection of γ-ray signals from Crab Nebula and Mrk 421.

Crab Nebula. The Crab Nebula is one of the most comprehensively studied celestial objects, and, in fact, the only undoubtedly recognized source of very high energy particles, $E \geq 1$ TeV, in the Galaxy. Up to the present, VHE γ-rays from this source have been observed by several groups, the most significant results being those obtained with the imaging Cherenkov technique.

During the period 1994/1995 the Crab Nebula was observed by the second HEGRA telescope in the ON/OFF mode with 20 min duration of individual runs. For the period October '94 - March '95 the total number of ON/OFF run pairs is 351. After the preliminary filtering procedure 272 runs survived, with a total number of 920320 events in the ON runs and 904764 events in the OFF runs, corresponding to 5440 min of ON observations of the Crab Nebula.

The basic parameters of the telescope CT-2 (effective collection areas, detection rates, energy threshold, γ/proton separation efficiency, etc.) were calculated using Monte Carlo simulations.

To eliminate the difference in sky brightness in the ON and OFF mode the "software padding lamps" approach is used. To exclude the influence of the night sky background and of the additional light from the star ζ Tauri in the FoV, the two-level "tail cut" procedure is applied. The second-moment image parameters are calculated. The comparison of Monte Carlo and measured distributions of image parameters shows good agreement.

The basic results of image analysis are presented in Table 1. The data analysis reveals a significant signal from the Crab Nebula at a level of $10\,\sigma$ during 90 hours of ON observations (see [3] for details concerning cuts and trigger conditions).

For the evaluation of the energy spectrum and the absolute flux of γ-rays by a single imaging Cherenkov telescope we use the method described in Ref. [4].

In order to determine the energy spectrum of primary γ-rays, the γ-ray acceptances κ_γ and detection rates R_γ^{MC} for different spectral indices and software trigger thresholds were calculated using the Monte Carlo simulations. Assuming a power-law primary spectrum, the spectral index can be estimated from a comparison of the measured detection rates, R_γ^{exp}, with the Monte Carlo detection rates, R_γ^{MC}. The results shows that the Crab spectrum is rather steep with an integral spectral index $\alpha_\gamma \simeq 1.7 \pm 0.1$ in the energy interval $1 - 3$ TeV. The measured spectrum agrees with the spectrum previously reported by the Whipple group. The γ-ray flux above 1 TeV is estimated as $F_\gamma(> 1\ TeV) \simeq 8 \pm 1 \pm 2.4 \cdot 10^{-12}$ photons/cm^{2}s.

The first term of uncertainties corresponds

Tab. 1: *Results of the data analysis for different software trigger conditions of "2/N" (at least two from N pixels) and regions of zenith angles of observations. Given are the numbers of events in the ON and OFF-source runs, and the significance of the difference signal.*

Parameter:	ON	OFF	ON-OFF	σ
2/19, $< 45°$				
Raw	148704	147932	772	1.4
Azwidth	4018	3550	468	5.4
Multicut	**2192**	**1718**	**474**	**7.6**
2/19, $< 30°$				
Multicut	**1587**	**1153**	**434**	**8.3**
2/37, $< 30°$				
Multicut	**2934**	**2221**	**713**	**10.0**

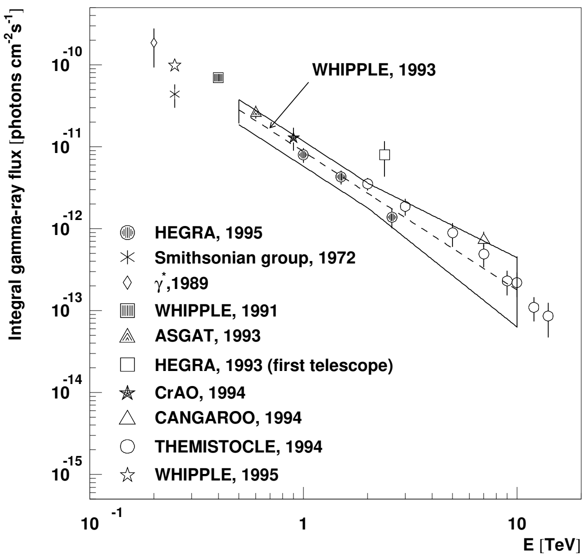

Abb. 1: *The integral γ-ray flux from the Crab.*

to a statistical error of $\sim$ 12%, and the second term corresponds to a systematic error of $\sim$ 30% [3].

The final result on the evaluated $\gamma-$ray flux from Crab Nebula is presented in Fig. 1.

Markarian 421. Markarian 421, an active galaxy at the distance $d \approx 100\,\mathrm{Mpc}$ (redshift z=0.031), has been detected at high confidence level by the Whipple collaboration in 1992-1995 at energies above a few hundred GeV.

Tab. 2: *Results on Markarian 421 data analysis.*

Cuts	ON	OFF	DIFF	σ
Orientation	3881	3648	233	2.7
Shape	3414	3071	343	4.3
Orientation+ Shape	2630	2329	301	4.3

Markarian 421 has been observed by CT-2 in December '94 - May '95.

After the standard procedure of event filtering (eliminating data with bad weather conditions, technical problems, etc.) 161 ON/OFF runs with a total "ON" observation time $t \approx 62\,\mathrm{h}$ have survived.

Basically, the data reduction procedure was the same as that used for the Crab Nebula. The data analysis reveals an excess of 300 ON events after application of the *Shape* as well as *Shape+Orientation* cuts (see Table 2). The corresponding signal to noise ratio is estimated $\geq 4\sigma$.

It is necessary to note that the signal has been obtained by optimization of the image cuts. In contrary to the analysis of the Crab data, the resulting cuts differ from the Monte Carlo predictions. In particular, the shape parameters *Width, Length* appear to be smaller than the "standard" ones from a point source in the center of the camera. A possible explanation of this effect could be, in principle, a very steep spectrum of γ-rays in this energy region or a cutoff in the primary spectrum near the energy threshold of the telescope ($\approx 1\,\mathrm{TeV}$). In addition, it seems that the orientational parameters like *Miss* do not work "properly".

Forthcoming observations of Markarian 421 in 1996 by 3 HEGRA Cherenkov telescopes will clarify whether these effects are the result of statistical fluctuations, or of possible technical problems during the observations of this source, or whether they have an "astrophysical" background.

2.2.3 The new HEGRA CT system

The HEGRA collaboration is installing a five-telescope IACT system on La Palma, based on telescope mounts and mirrors identical to those used for CT-2, but equipped with high-resolution, large field-of-view cameras and VME-based readout electronics, designed and built largely in Heidelberg. For a description of the camera and its associated electronics, we refer to last year's Annual Report. Most of the activities of the Heidelberg CT group in 1995 were devoted to the installation and commissioning of CT-3 – the first HEGRA telescope combining the large, alt-azimuth mounted mirror, and the high-resolution camera of the final design – and to the completion, installation, and debugging of the software required to steer the telescopes and to control the data acquisition.

Installation of CT-3 and its alignment. As planned, the mount of CT-3 was transferred from Munich to Heidelberg in February. At the same time the EN-workshop, H. Fuchs, B. Braun, B. Jenne, G. Kober, W. Korgel, R. Nett and S. Oedel and from the electronics side N. Bulian and M. Stein had finished the first high resolution camera with the read-out electronics. Fig. 3 illustrates a phase during camera assembly, Fig. 2 shows the complete camera with open lid. The full telescope was assembled, not only to get acquainted with the mechanics of such a big and movable instrument, but also to perform various tests to demonstrate the quality of the telescope.

The newly developed high resolution camera contains more than four times as many pixels as CT-2. This results in a corresponding increase in delicate high voltage and signal cables which had to be installed along the mount in a safe way not interfering with the motion of the telescope.

The completely equipped and operating camera proved that there is no pick-up or base line problem for all 271 channels. The motors driving the two axes of the telescope were the source of concern.

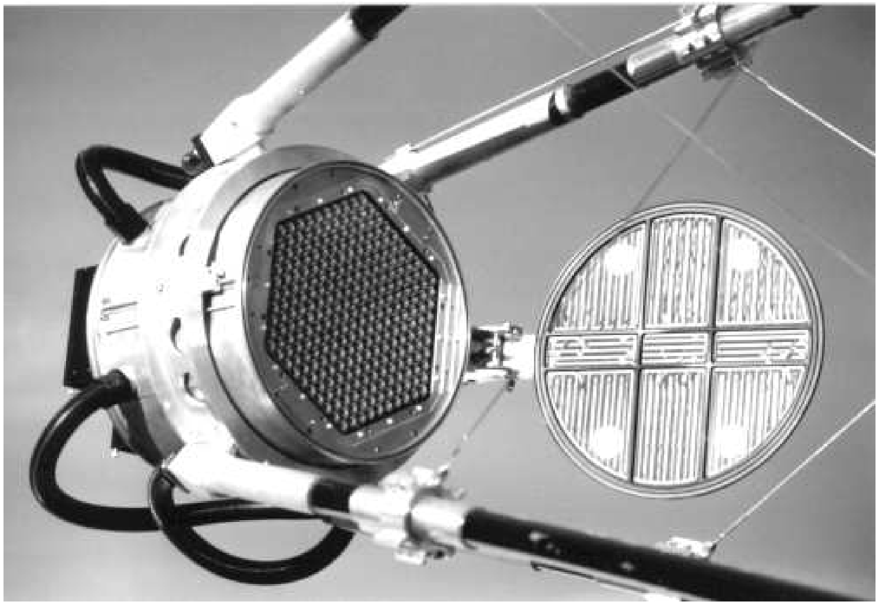

Abb. 2: *271-channel camera. View of the front side.*

The heat produced by the voltage dividers and the preamplifiers inside the camera had to be conducted away effectively.

In the new design the telescope drive is steered by the data acquisition computer via a commercially available VME module. The necessary tests were performed in Heidelberg as well.

When all tests were finished successfully, the telescope was dismantled and shipped to La Palma. In July it was reassembled at the central position of the telescope array and connected to the local computer network. Three weeks were enough to accomplish this task.

During the next two weeks the telescope was adjusted with great care. The azimuthal axis was aligned vertically to better than $0.01°$, the altitude axis horizontally with the same accuracy. Then the mirrors were adjusted one-by-one to provide a well-focussed image of a light source positioned in a distance of about one km; the camera was then shifted slightly to account for a typical distance of 6 to 8 km to the shower maximum as the Cherenkov light source. The optical quality of the telescope is such that a point light source is essentially imaged onto a single pixel. The precision of the telescope alignment and of the tracking was tested with stars of known location, and proved to be stable to less than 1/2 of a pixel diameter, both in the normal and reverse tracking modes.

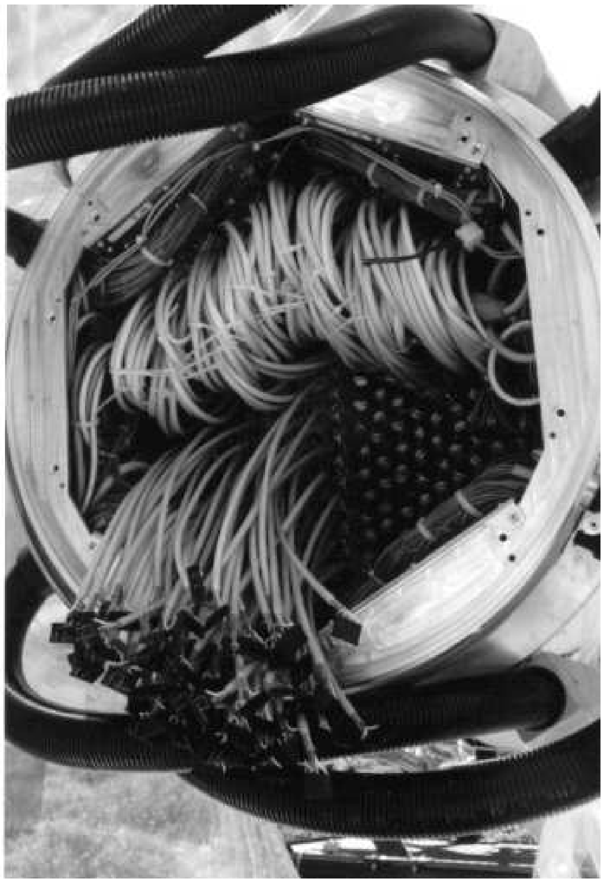

Abb. 3: *View of the back side of the camera during the installation of the PMT pixels.*

The online software. The online software of the system of telescopes was designed to:

- allow to operate a system of (moving) detectors by one person from a single terminal by the use of simple mouse click menus

- provide a graphical online display of events and telescope parameters
- perform an online event building to enable online monitoring of the performance of the system
- use modular processes for easy maintenance and modifications.

The architecture of the online software is illustrated in Fig. 4.

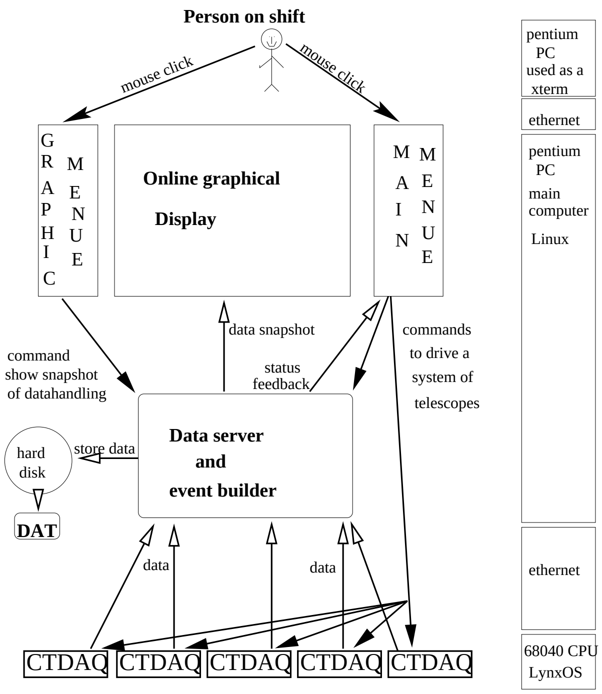

Abb. 4: *Architecture of the online software*

The key feature is a client/server structure with the local CPUs (68040) placed inside the VME electronic crates at each IACT, and a main Pentium PC server, running under Linux. The local CPUs, operating under LynxOS, load their software from the server host. Special partitions of the server's hard disk are accessible to the local CPUs via NFS.

The data acquisition software itself consists of a data server which receives data from each local "CTDAQ" process running on the local CPUs placed nearby each telescope. The server performs online event building, i.e. synchronization of data from several telescopes, and stores the synchronized data on disk. Contrary to the present CT-1/CT-2 system, where coincident events are assembled off-line, this feature allows the real-time monitoring of the performance of the CT system. The local "CTDAQ" processes have to perform several tasks in parallel (detector read-out, data pre-processing, network communication, telescope steering, service of user requests etc.) with the additional requirement to share data between tasks. The implementation makes use of "threads", which are a kind of unix subprocesses running within one main unix process, having access to the same stack.

One of the vital features of the online software is a second level software trigger, based on pattern recognition. Also, an online data sparsification is performed to reduce the amount of data per event from 4kbyte to approximately 1.5kbyte. During normal operation the rate of accepted events is of the order of 5Hz, leading to a deadtime $< 5\%$ and an expected total amount of 1-2 Gbyte of data for a 5 telescope system per night.

The system is controlled via a graphical user interface based on the "Tk/Tcl" language, and a graphical display based on the "vogl" library. Fig. 5 shows the online terminal during data taking.

The "Main" menu is dedicated to drive the whole system of telescopes from one terminal by easy mouse clicks. The actions caused by mouse clicks can be very complex, consisting of processes based on C-code, unix shell scripts, remote logins to other computers and command/data transfers via Ethernet UDP protocol. The menus adapt the disabled/enabled status of all buttons automatically, inhibiting disallowed command chains, and provide online help. The display also serves as an event display, controlled by a second menu, and a slow control monitor, showing error(red), warning (yellow) and ok (green) flags for various system parameters.

Presently, only a single telescope (CT-3) is controlled, but extensive laboratory tests were performed with multiple client CPUs, and we expect a smooth transition to the multi-telescopes system in 1996.

The steering of the telescopes. The steering of the telescopes is one of the most important features of the experiment, and a

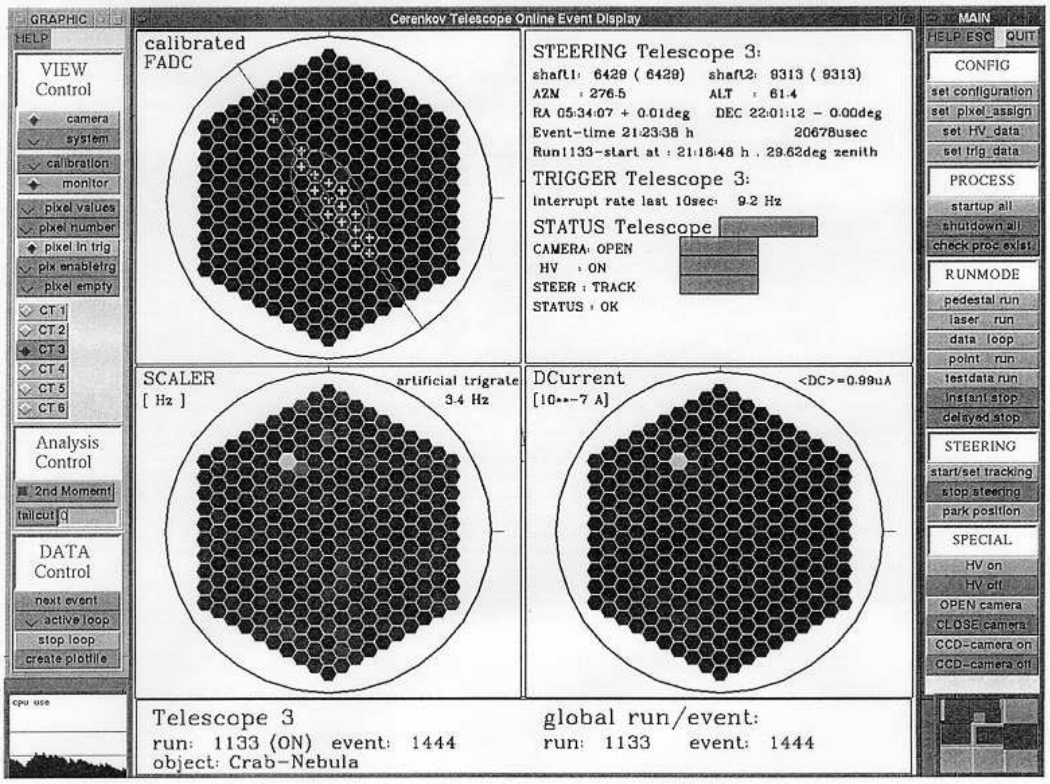

Abb. 5: *Online terminal view: graphical menu, online display, main menu*

new algorithm was developed for this purpose. The required accuracy is triggered by the Monte Carlo estimation of the 0.1° resolution in the reconstruction of the shower direction by the use of a five-telescope system. The azimuth-altitude mounts are controlled by two stepping motors of step size 0.0003°. The position of the telescopes is monitored by shaft encoders with a resolution of 0.02°. About 10 times per second, the algorithm is activated and determines the current position of the telescope from the shaft encoders, calculates the position and velocity of the object to be tracked, and adjusts the stepping speed in a way which avoids excessive acceleration of the telescopes as well as possible oscillation effects. The resulting tracking is good to one shaft encoder step, i.e. 0.02°.

Initial tests. The camera was equipped with 271 pixels, 2 of which showed problems during the first weeks and had to be exchanged. Apart from this initial problem, the camera did not require further maintenance during the following months of observations. Unlike the earlier telescopes, CT-3 is read out with a new FLASH-ADC system, allowing to reconstruct the shape and timing of the pulses. Since only 240 FADC channels were available, some channels near the periphery of the camera were not read out. For reliable operation, the FADC system was run at 100 MHz, slightly below the design values. The trigger for the readout is provided by a majority coincidence between camera pixels. The thresholds for the trigger discriminators were typically set to 18 mV, with 1.5 mV corresponding roughly to 1 photoelectron; single-pixel trigger rates averaged around 100 Hz, with a large spread between pixels. For typical night-sky conditions, a pixel current of about 800 nA was measured. A 2-fold coincidence was required to trigger the readout. The effective coincidence window was adjusted to 12 ns, minimized to reduce random triggers. In addition, a software condition was imposed passing only events where the two trigger pixels are neighbors, resulting in a data acquisition rate of 5 Hz.

To insure uniform and reproduceable trigger conditions, the laser calibration system was used to adjust all pixels to the same effective gain within 1.5% rms. The resulting pixel high voltages ranged between 640 and 920 V. Since the mean number of photons per laser pulse can be determined from the spread of the measured laser pulse heights (up to a O(20%) correction due to the width of the single-photon response), the laser data was also used to derive the conversion factors relating FADC counts to photoelectrons. Over periods of weeks, the PMTs were extremely stable, with the spread of gains growing only slightly to 2.6%. The typical electronics noise was measured to 0.5 photoelectrons with closed camera; with open camera, night-sky photons increased the noise to 1 photoelectron.

Trigger rates. After these initial tests and adjustments, attention turned to the study of trigger rates. Since, contrary to the earlier telescopes CT-1 and CT-2, the trigger signals are latched, CT-3 allows improved diagnostics. Reading only the trigger latches, additional software trigger criteria can be applied before the whole data are read out, such as requiring next-neighbor trigger pixels. With a decision time of only a few 100 μs, such filters reduce the rate of random coincidences very effectively, and allow the operation with lower thresholds on the individual pixels.

Fig. 6 illustrates the distribution in the number of pixels exceeding the trigger threshold.

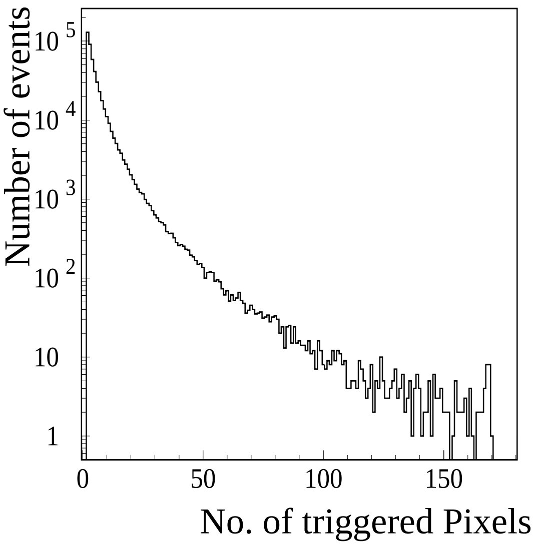

Abb. 6: *Distribution in the number of triggered pixels.*

The steeply falling spectrum reflects the spectrum of cosmic rays; most frequently, only two pixels trigger, but events with 150 and more trigger pixels are also observed. In order to find the optimum value for the pixel trigger threshold, thresholds between 15 mV and 35 mV were scanned. For a given threshold setting, the rate of random triggers is calculated based on the measured single-pixel trigger rates and the known coincidence time window. One aims for the lowest threshold where the fraction of random coincidences among all events is still small. The various measured rates are illustrated in Fig. 7.

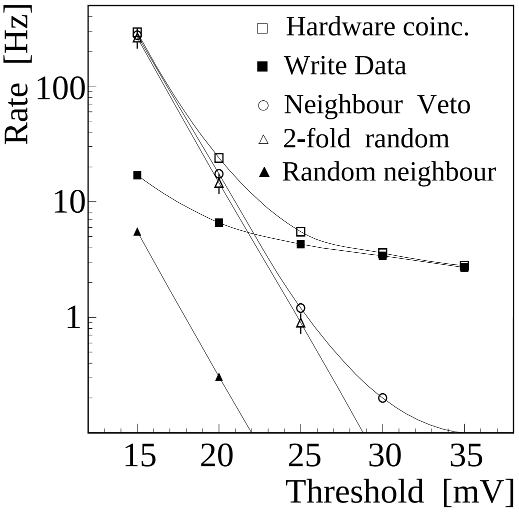

Abb. 7: *Trigger rates as a function of pixel trigger thresholds (1.5 mV is roughly equivalent to 1 photoelectron). Shown is the hardware two-pixel coincidence rate, the rate at which the software next-neighbor trigger rejects events, the final event rate, and the calculated random rates for the two-pixel trigger and the two-pixel, next-neighbor trigger.*

The hardware coincidence rate (“Hardware coinc.”) varies slowly for thresholds above 25 mV, and increases rapidly with lower thresholds. The calculated random trigger rates account well for this increase. Indeed, the software next-neighbor trigger rejects events at a rate consistent with the random rate (“Neighbor veto”); according to Monte-Carlo studies, it will reject less than 5% of good events. The rate of accepted events (“Write data”) exhibits a power-law dependence on the threshold, with a index of $\alpha \approx 1.5$, in close agreement with the integral spectral index of charged cosmic rays, $\alpha_{CR} \approx 1.7$. Only at thresholds well below 20 mV does the calculated random rate for the next-neighbor condition reach the 10%-level. Based on these data, the 18 mV trigger threshold was chosen.

Occasionally, a relatively bright star will be in the field of view of the camera. This is e.g. the case for observations of the Crab nebula, were Zeta-Tauri (about 1° from the Crab) is imaged onto one or two pixels, causing currents up to 45 μA, and pixel trigger rates up to 100 kHz.

Due to rotation of the field of view caused by the alt-azimuth mount, the star moves across the camera. Under such conditions, even the otherwise negligible next-neighbor random rate increases up to 50 Hz, meaning that most of the events written to tape are random triggers. Since the inclusion of pixels in the trigger is software-controlled, the data acquisition program was modified to dynamically exclude pixels with large currents from the trigger. With this change, less than 5% of all accepted triggers for Crab observations are due to random coincidences. Of course, the automatic changes in the trigger configuration are recorded, and identical trigger criteria can be applied offline to off-source data.

After stable stand-alone operation of CT-3 was achieved, the control software of CT-1 and CT-2 was modified in order to allow synchronized observations. Data are however still written to separate data streams, and events are synchronized off-line based on the event time. Given a 5 Hz trigger rate of CT-3, one finds a coincidence rate with at least one of the other telescopes of about 1.7 Hz. The rate of coincidences between CT-2 and CT-3 is about 1.5 Hz, the CT-1 $\cdot$ CT-3 rate is about 0.9 Hz, and all three telescopes trigger with a rate of about 0.7 Hz. An example of a coincident event is shown in Fig. 8.

Detailed analysis of such events is in progress. Major limiting factors are, however, the inferior cameras of CT-1 and CT-2, and the fact that the telescopes are almost arranged along a line, resulting in poor stereo imaging for showers with impact points near this line. Only with the additional telescopes and new cameras to be installed in 1996 will a good 3-dimensional reconstruction be feasible for a large fraction of all events.

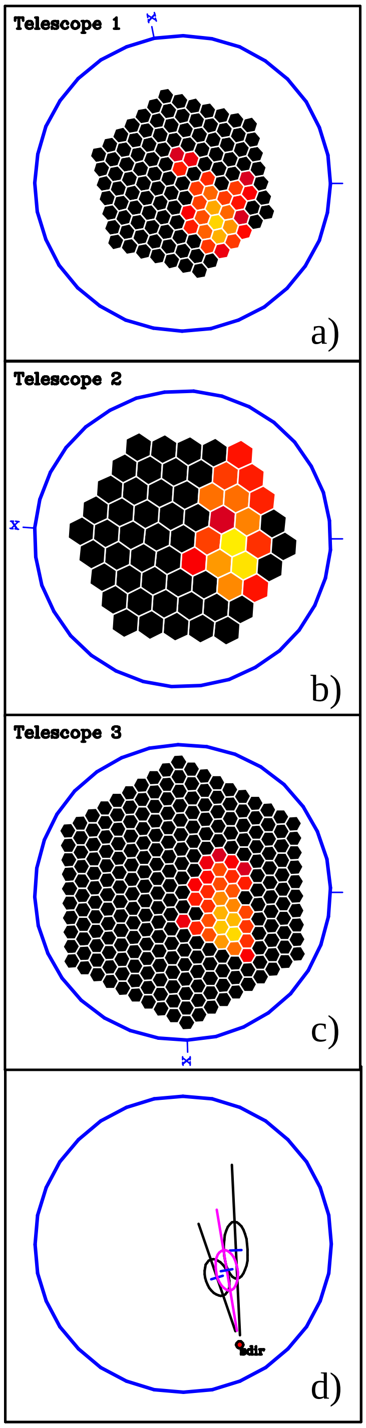

Abb. 8: *Coincident event as viewed in the cameras of CT-1 (a), CT-2 (b), and CT-3 (c). The shower axis (i.e., the image of the source) is reconstructed as the intersection of the long axes of the shower images (d).*

First observations of the Crab Nebula with CT-3. As part of the commissioning and as a final test, about 50 h of observations of the Crab Nebula were taken with CT-3 in 1995, equally shared between on-source and off-source runs. In total 700000 events were accumulated. At this time we can only present a very preliminary glance at the data.

The events were analyzed in the standard fashion, by calculating the second-moment image parameters (the width, length, and orientation of the shower image), and by applying cuts to enrich gamma-rays, which are characterized by compact, short and narrow images. Even with the rather modest amount of data, a clear signal quickly became visible. As an illustration, Fig. 9 shows the distributions in the angle α characterizing the orientation of the image. Since the telescope is pointing to the Crab Nebula, the images of showers from the direction of the Crab are oriented radially, pointing away from the camera center, with small values of α. Indeed, in the on-source data sample a clear excess is seen at small α, whereas the corresponding distribution in the off-source sample is flat.

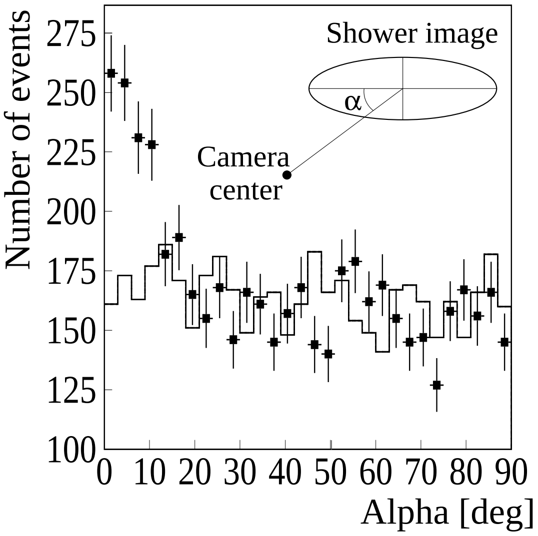

Abb. 9: *Distribution of the orientational parameter α for the on-source (dots) and off-source (solid line) data sample.*

While further conclusions will have to await a more quantitative analysis, this initial result is certainly quite promising.

Status of the HEGRA CT system. Since no major problems were revealed during the assembly and the first data taking of CT3, the production of the next telescopes was started with full force in autumn. The EN-workshop has finished most parts of the camera bodies and furnished the electronics containers. Work on the structures to hold the pixels, on the parts to guide the cable trees and the pixel production itself are well advanced. In the electronics workshop all electronics components from the preamplifier to the cable trees and the read-out electronics are being tested and assembled. The progress made there supports the confidence to complete the telescope system in 1996.

2.2.4 Hardware developments

In parallel to the construction of the camera, special hardware aspects were investigated in depth. We mention here the study of PMT properties and the work on mirror optics.

PMT trigger rates due to night-sky photons. The typical pixel trigger threshold of CT cameras, $q_\circ \approx 20...30$ photoelectrons, is very large compared to the mean number of less than one photoelectron per PMT integration interval. The conventional assumption was that pixels trigger due to statistical fluctuations in the number of photoelectrons, yet neither Poisson statistics nor the PMT-intrinsic width of the single-photoelectron peak suffice to explain why such a large trigger threshold is required to achieve manageable rates. A detailed laboratory study was conducted to investigate this issue, with PMTs illuminated by light sources of controlled intensity. It was found that in the relevant range of photon fluxes, the trigger rates rise linearly with the photoelectron rates, indicating that fluctuations in the single photoelectron response are responsible for the triggers, rather than multi-photoelectron overlap. Indeed, the single-photoelectron peak shows, at a level around 10^{-3}, a pronounced tail towards large pulse heights, ranging up to 20 times the mean signal per photoelectron and more (see Fig. 10). The level of the tail is very sensitve to the voltage between photocathode and first dynode, and insensitive to the voltages at later

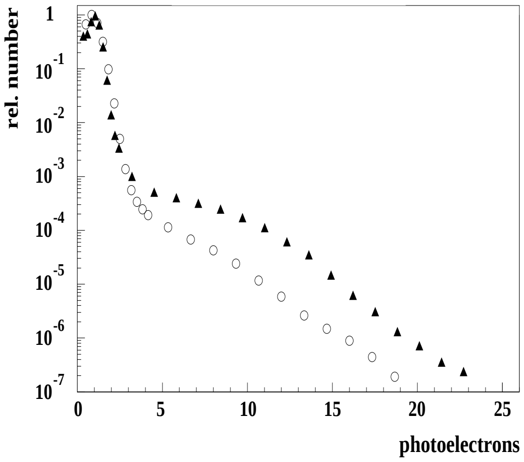

Abb. 10: *Charge spectrum obtained for low-level (single-photoelectron) illumination of the PMT, in terms of the mean charge per photoelectron. Data points refer to different voltages between cathode and 1st dynode: 140 V (circles) and 250 V (triangles).*

dynodes. A familiar phenomenon in PMTs is the ionization of residual gas atoms by photoelectrons, causing the generation of additional electrons when the ion hits the photocathode. The resulting, potentially large pulses should be delayed by the ion drift time of a few 100 ns compared to the primary photoelectron. Measurements with a fast pulsed light source did indeed show that the large pulses come about 500 ns after the light pulse, and that the large-amplitude tail was much reduced for prompt signals. These results - which are summarized in [5] - add new requirements for the selection of PMTs and the design of the voltage deviders; in particular, the voltage between cathode and 1st dynode should not be increased beyond the values required to achieve good electron collection.

Ray-tracing of the Cherenkov Telescopes. The reflector of the HEGRA Cherenkov telescopes [6] consists of 30 spherical glass mirrors, which differ - due to manufacturing tolerances - in their radius of curvature. The specified field of view extents to $\pm$ 2.5^o. The Cherenkov light from the shower - with its maximum $\sim$ 6-8 km above the site at La Palma - should be contained in one camera pixel of 0.25^o.

Due to the large angular acceptance of the telescope the formulae for aberrations derived in the paraxial limit are no longer valid. In addition they yield the maximum extent of the images only and do not quantify the light intensity in the image plane. Thus an optical ray-tracing program has been developed to investigate the performance and compare various optical designs chosen for Cherenkov telescopes. Also tolerances for the choice of a specific arrangement of mirrors having different radii of curvature have been determined as well as necessary mirror alignment accuracies.

The ray-tracing program employs a novel matrix approach for the reflection from individual spherical and parabolic mirrors. In a first step the validity of the program has been proved by comparing the results to those obtained from the classical Seidel aberrations in the paraxial limit. Then different layouts have been investigated for reflectors having the same diameter - - D = 388 cm - and focal length - f = 500 cm:

1. Monolithic reflector mirrors
   (a) with a spherical surface,
   (b) with a parabolic surface, as employed e.g. for the CANGAROO Cherenkov telescope.
2. Reflectors containing 30 spherical mirrors with 60 cm diameter,
   (a) the Davies-Cotton design, with all mirrors having identical focal length f arranged on a spherical reflector surface with a radius of curvature of f,
   (b) the HEGRA [7] design, where the mirrors in four radial zones have focal lengths differing by as much as ± 2 cm. A slight distortion of the spherical reflector shape had been originally suggested for optimum optical imaging.

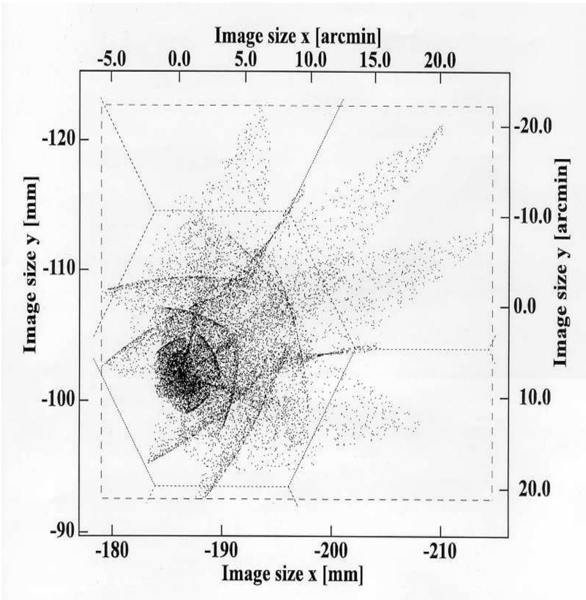

Abb. 11: *Optical performance of the HEGRA reflector design. The light intensity distribution evaluated at an image distance $z_0 = 4920$ mm is shown for an incident angle of $\vartheta = 2.5^o$. The dotted hexagons indicate the pixels of the camera.*

The two-dimensional light distribution from large reflectors in the image plane is quite complicated, especially at the edge of the field of view, as shown in Fig. 11 for the HEGRA layout. A parametrization of this distribution is not straightforward. Therefore we have determined the radius $r_{eq}(\eta)$ of a spherical aperture, which passes the fraction of light η.

For the four investigated reflector layouts similar results for r_{eq} are obtained even at the

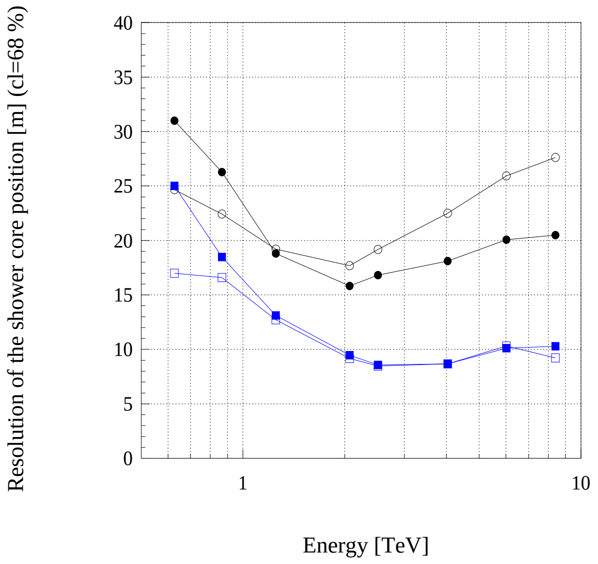

Abb. 12: *Resolution of the shower core position for the reconstruction by a second moment analysis (•) and the χ^2-fit (■) when only the triggered telescopes are used and when additional telescopes are used in the second moment analysis (∘) and the χ^2-fit (□) as function of energy of the γ-primary. The resolution is defined as the radius of a circle around the true position which contains 68 % of the reconstructed events.*

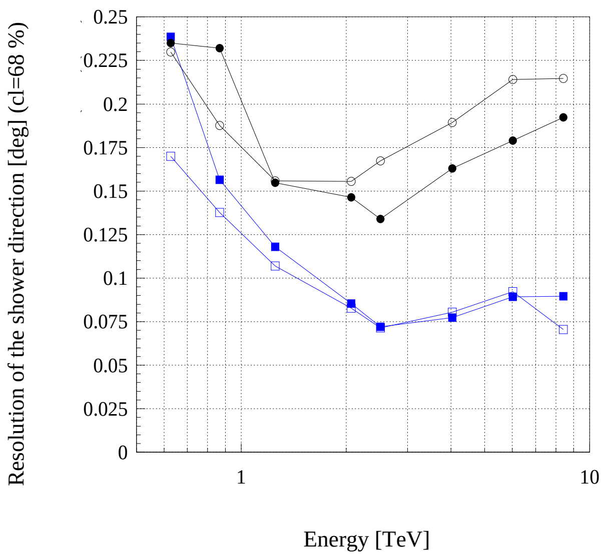

Abb. 13: *Resolution of the shower direction for the recontruction by a second moment analysis (•) and the χ^2-fit (■) when only the triggered telescopes are used and when additional telescopes are used in the second moment analysis (∘) and the χ^2-fit (□) as function of energy of the γ-primary.*

edge of the field of view i.e. for an angle of the incident light of $\vartheta = \pm 2.5^o$. In an assumed pixel size of 0.25^o a fraction $\eta = 95\%$ of the light is contained for the Davies-Cotton and the HEGRA design provided the appropriate image distance is chosen.

Detailed results on the mirror alignment tolerances, the choice of the focal lengths for the HEGRA design and finally the isochronicity are contained in [7].

2.2.5 Monte Carlo studies

Through the last years, significant emphasis has been placed on Monte Carlo studies to provide a deeper understanding of the properties of IACTs, to optimize the analysis technique, and to enlarge the physics scope. In the following, two specific examples are discussed.

A new technique for image analysis in a system of atmospheric Cherenkov telescopes. On the basis of simulations, the distribution of the light intensity produced by γ-ray showers in the focal plane of a Cherenkov telescope and its dependence on shower parameters have been modelled. This model is used in a χ^2-fit which yields an estimate for the location and direction of the axis, the height of the shower maximum and the energy of an individual shower. The images observed by the telescopes in the system are fitted simultaneously with respect to the shower parameters. In contrast to a second moment image analysis the χ^2-fit uses the full information about the shape of the image.

This fitting procedure [8] was applied to vertical γ-ray shower events simulated in different energy intervals ranging from 500 GeV to 10 TeV. The system of five IACTs was simulated, with telescopes arranged on the corners and in the center of a square where the telescopes on the corners have 85 m distance. Each telescope has a 271 pixel camera with 0.25^0 pixel size. The trigger criterion for one telescope requires that at least 2 out of 271 (2/271) pixels exceed a threshold of $q_0 = 10$ ph.e and two of them are next neighbours (NN). At least 2 telescopes of the system (2/5) should trigger.

The results of this application shows that the reconstruction of the shower core position by the χ^2-fit provides an improved resolution in the whole energy region from 0.5 to 10 TeV relevant for the IACT. At the threshold of the IACT of around 800 GeV the reconstruction of the impact point on ground is improved through the χ^2-fit by 30 %, and at energies higher than 2 TeV by more than a factor of 2 (Fig. 12). At energies below 2 TeV the resolution is dominated by photon statistics. The same behaviour can be seen in the determination of the shower direction (Fig. 13). The direction of a 1 TeV γ-ray can be reconstructed with an accuracy of 0.12^0.

At threshold an additional improvement of around 15 % in the resolution of the core position and of the direction is achieved by using even the recorded images in the telescopes which have, without triggering, at least 20 photoelectrons collected in their camera (see Figs. 12 and 13).

Finally, the penetration depth of the shower maximum can be reconstructed with a resolution of about 1 radiation length at threshold and the energy is estimated with roughly 20 % accuracy by the χ^2-fit with an overall additional systematic error of less than 10 %.

Monte Carlo study of the possibility to measure the cosmic ray spectrum using CT-3. It is quite possible that the imaging atmospheric Cherenkov technique holds the best promise for the study of the primary cosmic radiation in the energy region from 1 TeV to several tens of TeV. This energy domain of CRs is below the threshold of the standard air shower arrays. At the same time relatively low CR fluxes require large collection areas which makes balloon and even satellite experiments not very effective. The imaging CT technique may provide not only high detection rates (see Fig. 14), but also effectively identify primary nuclei exploiting the angular distribution of the Cherenkov light of atmospheric showers (see Fig. 15).

The simulations include detection of vertical air showers initiated by the primary proton and nuclei from different groups in the energy range 100 GeV - 100 TeV by a single HEGRA telescope like CT-3 described in Sec.2.2.3.

The maximum of the shower development is higher for heavy primary particles; correspondingly, the density of the Cherenkov photons at the observation level is low due to the angular extension and atmospheric attenuation. Therefore air showers initiated by light nuclei (p, He) have larger collection areas, and corresponding

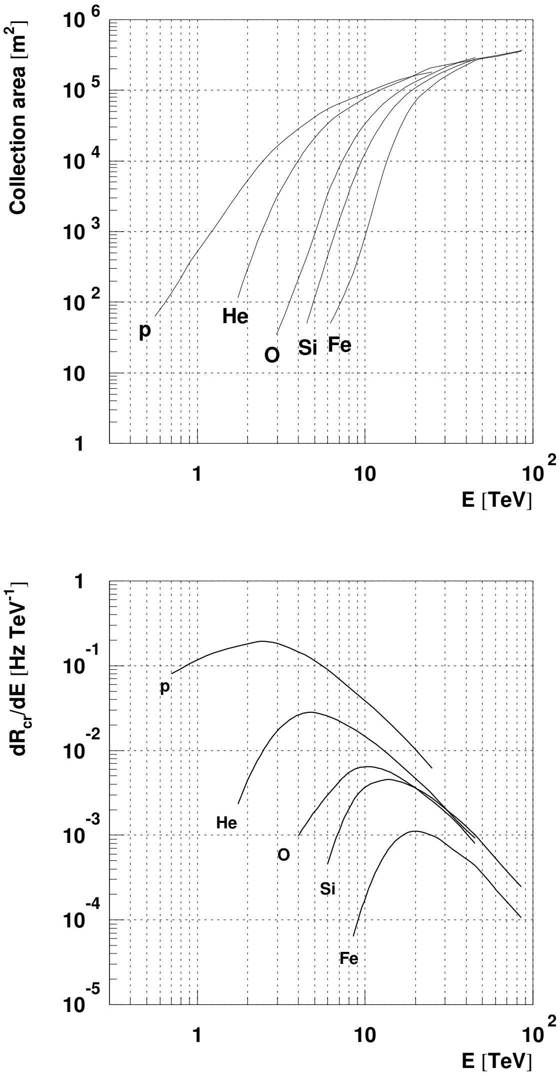

Abb. 14: *The collection areas and differential detection rates of proton and nuclei initiated air showers.*

ly higher detection rates, especially at energies $E \leq 10\,\mathrm{TeV}$.

The energy E^* corresponding to the maximum of the differential detection rates depends on the atomic weight A as $E^* \propto A^\beta$, where $\beta \approx 0.5$. The relative integral detection rates of primary nuclei (normalised to that of primary protons), calculated for the "standard" CR composition, are the following: He - 0.25; CNO (O) - 0.11; Ne-Si (Si) - 0.1; Fe - 0.03.

For the identification of different components of CRs the following classification parameters could be used: (i) standard image shape parameters *Width, Length*, (ii) *image size, s* (total number of photoelectrons in the Cherenkov light image); (iii) *image density, d=s/n* (average number of photoelectrons that is con-

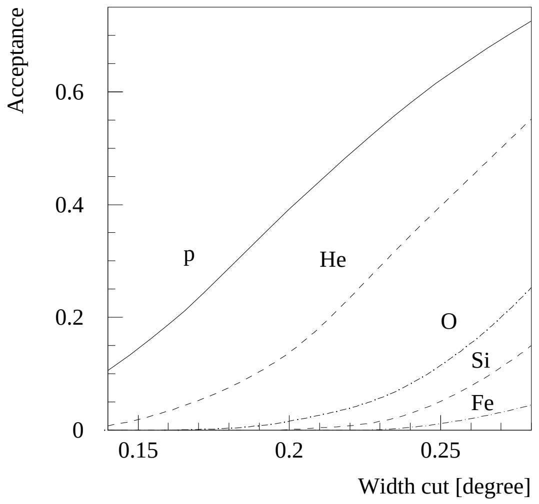

Abb. 15: *Acceptance of Cherenkov light images detected from air showers initiated by the given different primary nuclei, applying the standard Width cut.*

tained in one image pixel used for the image parametrization); (iv) χ^2 *criterion* (measure of the image fluctuations along the major and minor axis).

Figs. 14 and 15 show that the application of the single, but very effective parameter *Width*, is already sufficient to remove effectively the contributions from all nuclei, including α-particles, and thus to measure the energy spectrum of the alone proton component. These measurements are of special interest for the theory of acceleration of galactic CRs since they may examine the possible indication from recent MUBEE and JACEE balloon experiments about a strong steepening of the proton spectrum above several TeV. Hopefully the data obtained by CT-3 in 1996 will be sufficient for such study.

It is hoped that the system of 5 HEGRA telescopes will allow us not only to essentially improve the spectral measurements of the proton component of cosmic rays, but also to study the fluxes and spectra of different groups (p, He, (CNO), Ne, Fe) of CR nuclei.

References:

[1] Mirzoyan R. et al. *NIM* **A351**, 513, 1994.
[2] Jahresbericht MPIK Heidelberg 1994, p. 75.
[3] Konopelko A. et al., *Astroparticle Physics*, in press, MPI-H-V42-1995.
[4] Aharonian F. et al. *J. Phys. G: Nucl. Part. Phys.* **21**, 419, 1995.
[5] Hermann G. et al. MPI H-V36-1995, 1995.
[6] Aharonian F. et al. Proposal for Imaging Air Cherenkov Telescopes in the HEGRA Particle Array, Kiel 1989 (unpublished).
[7] Akhperjanian A. et al. The Optical Layout of the HEGRA Cherenkov Telescopes, Heidelberg 1995, Technical Report No. MPI-H-V46-1995
[8] Ulrich M. *"Towards a Major Atmospheric Cherenkov Detector - IV"*, Padova, Italy, 1995.